

3D CARDIAC MOTION TRACKING USING ROBUST POINT MATCHING AND MESHLESS DEFORMABLE MODELS

Ting Chen¹, Xiaoxu Wang², Dimitris Metaxas², Leon Axel¹

Radiology Department, New York University¹
CBIM Center, Computer Science Department, Rutgers, the State University of New Jersey²

ABSTRACT

We propose a novel 3D motion estimation approach integrating the Robust Point Matching (RPM) and meshless deformable models. In our study, we first use the Gabor filters to generate phase maps of Short Axis (SA) and Long Axis (LA) tagged MRI sequences. Then we use the RPM to track the heart motion sparsely at intersections of tag grids in these image sequences, using both intensity gradient and phase information. Next, the new meshless deformable model is used to recover the dense 3D motion of the myocardium temporally during the cardiac cycle. The deformable model is driven by external forces computed at tag intersections based on the RPM motion tracking and keeps a consistent but flexible topology during the deformation using internal constraint forces calculated by the Moving Least Squares (MLS) method. The deformable model recovers the global deformation of the LV such as rotation, contraction and twisting by integrating global deformation parameters over the volume. The new model avoids the singularity problem of mesh-based deformable models and is capable of tracking deformation efficiently with the sparse external forces derived from tagging line intersections. We test the performance of the new approach on *in vivo* heart data of healthy subjects and patients. The experimental results show that our new method can fully recover the myocardium motion and strain in 3D.

Index Terms— Motion measurement, tracking, modeling.

1. INTRODUCTION

Tagged Magnetic Resonance Imaging (tMRI) [1] is a non-invasive way to track the *in vivo* myocardial motion during cardiac cycles. tMRI data is acquired by creating regional magnetic perturbations in the object, which are displayed in MR image as stripe-like darker tag structures embedded in relatively brighter myocardium. Tags are material properties so that they deform as the heart contracts and relaxes during the cardiac cycle. Myocardial motion in one direction can be quantitatively measured by tracking the deformation of tags that are initially in the perpendicular direction. For heart study, usually tags were created in three sets of mutually

orthogonal tag planes, two of which are perpendicular to the short axis (SA) image plane and one to the long axis (LA), to form 2D tag grids in the myocardium for both views of the heart. Using appropriate mathematical approaches, we can retrieve 2D displacement fields in these image planes by tracking the deformation of tag grids. Compared to the conventional MRI, which can only capture the global cardiac function measurements such as the ventricular volumes, tagged MRI can be utilized to recover local heart wall motion within the myocardium and derive critical clinical information such as strain.

Previously, a motion tracking method based on the use of Gabor filters bank and the RPM has been proposed [2] [3] to capture the myocardial motion in tMRI. The major limitation of the method is that it is a 2D approach. In addition, the FEM-based reconstruction of the dense displacement field has the problem of element degeneration.

Deformable models have been widely used for the 3D cardiac motion reconstruction from tagged MRI. Park et al. [4] [5] [6], Haber et al. [7], and Park et al. [8] [9] designed deformable models with global parameter functions to recover the LV and right ventricle (RV) motion. Spline models have also been developed to describe the motion of LV in [10]. These models are mesh-based and their deformation is computed using Finite Element Method (FEM). The mesh structure, however, may limit the performance of deformable models because the lack of topology flexibility and the generation of singularity during large deformation. Usually, mesh-based deformable models require re-meshing during the deformation, but this procedure is tedious and does not always guarantee returning a mesh with the optimal structure. Meshfree particle methods, which are also known as meshless methods, were first introduced to deal with the modeling of objects with cracks and surface discontinuities [11] and have been later applied in graphical motion simulation [12] [13] [14]. The meshless method simulates the motion of an object by computing the motion at a set of discrete points inside the object boundary with Smoothed Particle Hydrodynamics (SPH) method [15]. The structure of the object is sustained during the deformation using the internal

constraint calculated by the Moving Least Square method [16].

To avoid mesh element degeneration and to efficiently address the problem of large deformation tracking, we propose a new 3D motion tracking method integrating the RPM, the meshless method, and the deformable model [17]. We use the new method for 3D cardiac motion reconstruction from tMRI data. In the 3D motion reconstruction procedure, motion at tag intersections in SA and LA are first tracked using the RPM and Gabor filters. Then we construct a meshless deformable model composed of particles. The tag intersections are used as control points of the model, where external forces are calculated based on displacement and redistributed to particles throughout the object. The internal force at each particle is computed using the MLS method to simulate the elasticity of the myocardium. The model evolves in 3D following the Lagrange equation, driven by both the external and internal forces.

We demonstrated the strength of the new approach for 3D cardiac motion reconstruction from tMRI by testing its performance on *in vivo* cardiac images. The experimental results showed a good convergence between our dense motion reconstruction and the ground truth tMRI. Moreover, the analysis revealed the difference between normal and pathological cardiac motion.

Our paper is organized as follows: section 2 introduces the framework of the new motion tracking method; section 3 presents the deformation results on a numerical phantom and then elaborates its medical application on tagged MRI analysis; and in section 4 we draw the conclusions.

2. METHODS

2.1. Sparse Motion Tracking

The motion tracking process starts with the segmentation of the myocardium around LV in tagged MR images. We use the method developed in [18] for the delineation of myocardial boundaries. A previously constructed 3D shell model of heart is registered to the image space using landmark points on the myocardial boundaries. The region within the intersection of the shell model and the 2D image plane is assumed as the myocardium in 2D tMRI.

Given a cardiac tMRI sequence and the segmentation of the myocardium around the LV in all frames, we start the motion tracking by using the Gabor filters bank to generate two phase-maps for each frame, corresponding to vertical or horizontal tags, respectively. Tag intersections can be easily located by finding local minima in the summation of phase maps. Only intersections that are within the myocardial region will be used in the following steps.

Given two sets of tag intersections X and Y in two different frames of the same image sequence, we can track the displacement between intersections in these two frames

by building a correspondence matrix \mathbf{Z} to correlate X and Y . According to the definition of Thin Plate Splines (TPS), \mathbf{Z} and the displacement function $f: R^2 \rightarrow R^2$ can be computed simultaneously by the minimization of the thin plate spline energy:

$$E_{tps} = \sum_{j=1}^M \sum_{k=1}^N z_{jk} \|y_k - f(x_j)\|^2 + \lambda \iint \left[\left(\frac{\partial^2 f}{\partial x^2} \right) + 2 \left(\frac{\partial^2 f}{\partial x \partial y} \right) + \left(\frac{\partial^2 f}{\partial y^2} \right) \right] dx dy \quad (1)$$

where z_{jk} are elements of the correlation matrix \mathbf{Z} , such that $z_{jk} = \frac{1}{T} \exp(-\|y_k - x_j\|^2 / 2T)$ satisfies $\sum_{j=1}^{M+1} z_{jk} = 1$ for $k=1, 2, \dots, N$ and $\sum_{k=1}^{N+1} z_{jk} = 1$ for $j=1, 2, \dots, M$ with $y_{jk} \in [0, 1]$. According to deterministic annealing, we add another entropy term $\sum_{j=1}^M \sum_{k=1}^N z_{jk} \log z_{jk}$ to the right side of equation [1]. As the temperature variable T decreases, elements in \mathbf{Z} will change from fuzzy to binary classifiers. f is the function of deformation and the second term on the right hand side of (1) is the TPS energy, with λ the weight.

To find \mathbf{Z} and f that minimize E_{tps} , we separate the affine and non-affine space using a QR decomposition of X , in which

$$X = [Q_1 | Q_2] \begin{bmatrix} R \\ 0 \end{bmatrix} \quad (2)$$

where Q_1 and Q_2 are M by 3 and M by $M-3$ orthogonal matrices, respectively. R is an upper triangular matrix that depicts the orientation of X . Allowing that $Y_{new} = \mathbf{Z}Y_{old}$ during the point matching process, we can rewrite the equation (1) in the following form:

$$E_{tps} = \|Q_2^T Y - Q_2^T \phi Q_2 \gamma\|^2 + \|Q_1^T Y - R d - Q_1^T \phi Q_2 \gamma\|^2 + \lambda \gamma^T Q_2^T \phi Q_2 \gamma \quad (3)$$

where $c = Q_2 \gamma$ is the non-affine deformation of X , d is the affine translation matrix. We can solve d and c in consequential order by letting the derivative of the right side of the equation (3) to be 0. We then compute the displacement function f using c and d , and the solution for \mathbf{Z} is easy given f . Note that this process may overestimate the non-affine displacement and cause an isotropic-structured X to flip after the deformation. To avoid that, we set a loose constraint on d to make it close to an identity matrix in order to reject dramatic global translation, and we set an upper threshold on the absolute value of elements in c to prevent the flipping.

2.2. Meshless Deformable Model

The TPS-based RPM can provide us point-to-point correspondence between tag intersections throughout the

cardiac cycle. However, such correspondence only exists in a 2D image plane and it is sparse compared to the image resolution. To fully extend our method into 3D, we integrate the idea of meshless methods into 3D deformable models.

In the new meshless deformable model, the object of interest is discretized into particles without a connecting mesh. Each particle and its neighboring particles can be viewed as a phyxel. Physical properties, such as mass, are distributed in the phyxel using a kernel function. The motion pattern shared by all particles can be described as global deformation, such as rigid transformation, scaling and twisting. We interpret the model-centered coordinates in a polar coordinate system or a cylindrical coordinate system, which has a few parameters indicating the global features of the model. Here we use the polar coordinates as our example. The model-centered coordinates of a particle can be written in the polar coordinates (α, β, ω) .

$$e = \omega a_0 \begin{pmatrix} a_1 \cos(\alpha) \cos(\beta) \\ a_2 \cos(\alpha) \sin(\beta) \\ a_3 \sin(\alpha) \end{pmatrix}$$

where $\alpha \in [-0.5\pi, 0.5\pi]$ varies vertically, $\beta \in [-\pi, \pi]$ varies horizontally, the transmural factor $\omega \in (0, 1]$ is the ratio of the distance from the point to the origin and the radius, and a_i are scaling parameters. For LV modeling, usually we define $\alpha \in [-0.5\pi, 0.25\pi]$ from apex to the base of the LV, $\beta \in [-\pi, \pi]$ is horizontal, starting and ending at the inferior junction of LV and RV.

The model deforms following the Lagrange equation:

$$\mathbf{D}\dot{\mathbf{x}} = \mathbf{f}_{ext} + \mathbf{f}_{int} \quad (4)$$

where the damping matrix \mathbf{D} is the identity matrix in our case. The external forces are applied at tag intersections and redistributed over the model.

The external forces on each particles are transformed to the forces on global parameters $(a_0, a_1, a_2, a_3, \tau)$, where τ represents rotation. The forces on global parameters are integrated over the whole object to compute the velocity of the global parameters. At each time step, the global deformation of the model is recalculated using updated global parameters.

The internal forces are calculated locally using MLS. MLS minimizes the weighted difference between the observed displacement and the displacement approximated by its neighbors with first order accuracy:

$$e = \sum_j (\tilde{u}_j - u_j)^2 w_{ij} \quad (5)$$

where $\tilde{u}_j = u_i + x_{ij}^T \nabla u|_i$, w_{ij} is the interaction weight computed using the kernel function. Components of the displacement gradient ∇u at node i can be computed as (for example, the x component):

$$\nabla u_x|_i = A^{-1} \sum_j (u_j - u_i) x_{ij} w_{ij} \quad (6)$$

where $A = \sum_j x_{ij} x_{ij}^T w_{ij}$.

Next we compute the local strain energy using:

$$U_i = v_i \frac{1}{2} (\sigma_i \cdot \varepsilon_i) \quad (7)$$

where v , σ , and ε are the volume of the phyxel, the stress, and the strain, respectively. The force at particle j caused by deformation at particle i can be computed by

$$f_j = v_i \sigma_i \nabla_{u_j} U_i \quad (8)$$

The internal force at a particle i is the sum of counter forces at particle j in its neighborhood (phyxel).

$$f_{int}|_i = -\sum_j f_j \quad (9)$$

3. EXPERIMENTS

We tested the method on *in vivo* tMRI heart data. Tagged MR images were obtained from a Siemens Trio 3T MR scanner with 2D grid tagging. The 3D tagged MR image set we used consisted of a stack of 8 SA image sequence equally spaced from the base to the apex of LV, and 3 LA images, which are parallel to the long axis (LA) and with 60 degrees angles in between, as shown in Figure 1. The tag intersections in 2D images are tracked using RPM. The point tracking results are shown in Figure 2.

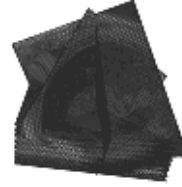


Figure 1: LV tMRI setting: 3 LA images

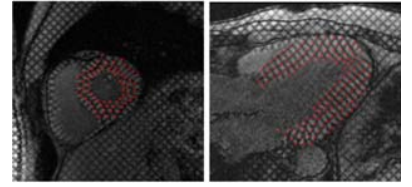


Figure 2: The intersections of grid tagging lines tracked by RPM.

The SA and LA images are registered using the spatial information in the DICOM header file. The endo- and epi-surfaces of the myocardium around the LV are delineated using a boosting method developed in [17]. Then the 3D model is registered to the image domain using landmark points on the contour of the heart. The tag intersections are tracked using the RPM to recreate displacement in 2D images as described in detail in [2] [3]. The 3D reconstruction results of a normal heart and a hypertrophic heart are shown in Figure 4 and Figure 5, respectively. We validated the method by using the tracked motion to compute myocardial strain, and compared the result against the ground truth on a numerical phantom. The RMS error of the method as well as other motion tracking methods, including HARP, are shown in Figure 3.

4. CONCLUSIONS

We developed a novel 3D myocardium motion tracking method for *in vivo* myocardial strain analysis. The method

can track 3D motion with high accuracy, using a meshless deformable model that can handle the complex shape and motion of the myocardium. The TPS-based motion tracking at tag intersections has been used to provide external forces for the deformable model, which speeds up the overall timing performance and sets an implicit global motion constraint for the deformable model. Internal forces at local particles are calculated using the MLS to avoid the singularity problem of mesh-based deformable models. In the future, we will apply the method to more heart data in order to quantitatively measure the difference between healthy and pathological hearts caused by heart disease.

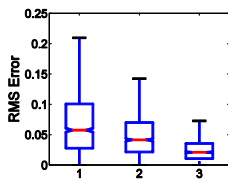


Figure 3: The RMS error of calculated strain against the ground truth on a numerical phantom. 1) error of HARP, 2) error of original deformable model based on Gabor filters, 3) error of the proposed method.

REFERENCES

- [1] L. Axel and L. Dougherty, MR imaging of motion with spatial modulation of magnetization, *Radiology*, 171, 841-845, 1989
- [2] T. Chen, S. Chung, and L. Axel, Automated tag tracking using gabor filter bank, robust point matching, and deformable models, in *Proceedings of Functional Imaging and Modeling of the Heart*, 22-31, 2007
- [3] T. Chen, S. Chung, and L. Axel, 2D motion analysis of long axis cardiac tagged MRI, in *Proceedings of Medical Image Computing and Computer-Assisted Intervention*, 469-476, 2007
- [4] J. Park, D. Metaxas, and L. Axel, Volumetric Deformable Models with Parameter Functions: A New Approach to the 3D Motion Analysis of the LV from MRI-SPAMM, in *proceedings of ICCV*, 700-705, 1995
- [5] J. Park, D. Metaxas, and L. Axel, Deformable models with parameter functions for cardiac motion analysis, *IEEE Transactions on Medical Imaging* 15 (3), 278-289, 1996
- [6] J. Park, D. Metaxas, and L. Axel, A finite element model for functional analysis of 4D cardiac-tagged MR images, in *Proceedings of Medical Image Computing and Computer-Assisted Intervention*, 491-498, 2003
- [7] E. Haber, D. Metaxas, and L. Axel, Motion analysis of the right ventricle from the MRI images, in *Proceedings of Medical Image Computing and Computer-Assisted Intervention*, 177-188, 1998
- [8] K. Park, D. Metaxas, and L. Axel, LV-RV shape modeling based on a blended parameterized model, in *Proceedings of Medical Image Computing and Computer-Assisted Intervention*, 753-761, 2002
- [9] K. Park, D. Metaxas, and L. Axel, A finite element model for functional analysis of 4D cardiac-tagged MR images, in *Proceedings of Medical Image Computing and Computer-Assisted Intervention*, 491-498, 2003
- [10] J. Declerck and J. Feldmar and N. Ayache, Definition of a 4D continuous planispheric transform for the tracking and the analysis of the LV motion, *Medical Image Analysis*, 197-213, 1998
- [11] T. Belytschko, Y. Krongauz, D. Organ, M. Fleming, and P. Krysl, Meshless methods: an overview and recent developments, *Computer Methods in Applied Mechanics and Engineering*, 3-47, 1996
- [12] M. Muller, R. Keiser, A. Nealen, M. Pauly, M. Gross, and M. Alexa, Point based animation of elastic, plastic and melting objects, in *Proceedings of the 2004 ACM SIGGRAPH/Eurographics symposium on Computer animation*, 141-151, 2004
- [13] M. Muller, D. Charypar, and M. Gross, Particle-based fluid simulation for interactive applications, *2003 ACM SIGGRAPH*, 154-159, 2003
- [14] J. Choi, A. Szymczak, G. Turk, and I. Essa, Element-free elastic models for volume fitting and capture, in *Proceedings of Computer Vision and Pattern Recognition*, 2245-2252, 2005
- [15] M. Desbrun and M. P. Cani, Smoothed particles: A new paradigm for animating highly deformable bodies, in *Proc. of the 6th Eurographics Workshop on Computer Animation and Simulation*, 61-71, 1996
- [16] P. Lancaster and K. Salkauskas, Surfaces generated by moving least squares methods, *Mathematics of Computation*, 141-158, 1981
- [17] D. Metaxas and D. Terzopoulos, Dynamic 3D Models with local and global deformations: deformable superquadrics, *IEEE Transaction on Pattern Analysis Machine Intelligence*, vol(13), 703-714, 1991
- [18] Z. Qian, D. Metaxas and L. Axel, Boosting and nonparametric based tracking of tagged MRI cardiac boundaries, in *Proceedings of Medical Image Computing and Computer-Assisted Intervention*, 636-644, 2006

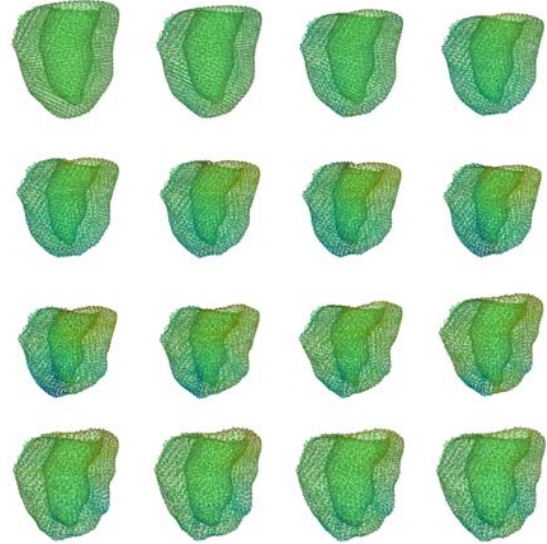


Figure 4: 3D motion reconstruction of a normal heart. It starts from end diastole and ends at 0.7 heart beating cycle.

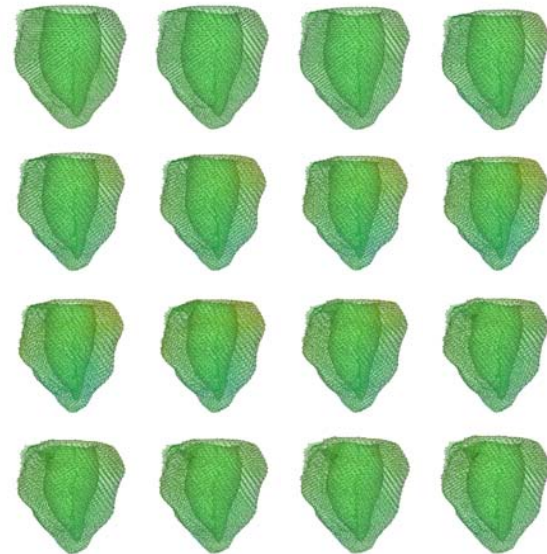


Figure 5: 3D motion reconstruction of the heart of a LVH patient. It starts from end diastole and ends at 0.7 heart beating cycle. Notice that the motion is relatively smaller in magnitude compared with normal heart.